1   **Response and biophysical regulation of carbon dioxide fluxes to climate variability and**

2   **anomaly in contrasting ecosystems in northwestern Ohio, USA**

3   Housen Chu[a, b, *], Jiquan Chen[a, c, d], Johan F. Gottgens[a], Ankur R. Desai[e], Zutao Ouyang[a, c, d],

4   Song S. Qian[a]

5

6   [a]Department of Environmental Sciences, University of Toledo, 2801 W. Bancroft, Toledo, Ohio

7   43606, USA

8   [b]Department of Environmental Sciences, Policy, and Management University of California,

9   Berkeley, 130 Mulford Hall, Berkeley, California, 94720, USA

10   [c]Center for Global Change and Earth Observations, Michigan State University, 218 Manly Miles

11   Building, 1405 S. Harrison Road, East Lansing, Michigan 48823, USA

12   [d]Department of Geography, Geography Building, 673 Auditorium Rd, East Lansing, Michigan

13   48824, USA

14   [e]Department of Atmospheric and Oceanic Sciences, University of Wisconsin-Madison, 1225 W

15   Dayton St, Madison, Wisconsin 53706, USA

16

17   [*]**Corresponding author:** Housen Chu

18   **Present Address:** University of California, Berkeley, Department of Environmental Sciences,

19   Policy, and Management, 130 Mulford Hall, Berkeley, California, 94720, USA

20   **Email:** hchu@berkeley.edu, **Phone:** 510-642-9048

Abstract

Recent climate variability and anomaly in the Great Lakes region provided a valuable opportunity in examining the response and regulation of ecosystem carbon cycling across different ecosystems. A simple Bayesian hierarchical model was developed and fitted against three-year (2011–2013) net ecosystem CO_2 exchange (F_{CO2}) data observed at three eddy-covariance sites (i.e., a deciduous woodland, a cropland, and a marsh) in northwestern Ohio. The model was designed to partition the variation of gross ecosystem production (GEP), ecosystem respiration (ER) and F_{CO2} that resulted directly from the short-term environmental forcing (i.e., direct effect) and indirectly from the changes of ecosystem functional traits (e.g., structural, physiological, and phenological traits) (i.e., indirect effect). Interannual variation of F_{CO2} was mainly driven by indirect effects, accounting for 54%, 89%, and 86% of the interannual variation at the woodland, cropland, and marsh sites, respectively. On the other hand, direct climatic effects accounted for 33% of interannual F_{CO2} variation at the woodland site and became irrelevant (<10%) at the cropland and marsh sites. In general, annual GEP and ER at each site tended to co-vary and dampen the interannual variability in F_{CO2}. Yet, year-to-year changes of GEP and ER were not spatially synchronous, suggesting that the ecosystem's response to climate was strongly site-specific in terms of the annual net CO_2 uptake. Future research should focus on the disparate response among ecosystems and develop a suitable framework to examine the mechanisms that drive differences in closely co-located ecosystems.

40 **Highlights**

41 1. Indirect effects drive the majority of interannual variability in CO_2 fluxes

42 2. Annual GEP and ER co-vary and dampen the variability in annual CO_2 uptake

43 3. CO_2 fluxes respond differently to similar climate conditions in co-located ecosystems

44

45 **Keywords**

46 Functional change, Interannual variability, Net ecosystem exchange, Climate anomaly

1. Introduction

Net ecosystem CO_2 exchange (F_{CO2}), which is the balance of two large and opposite carbon fluxes—gross ecosystem production (GEP) and ecosystem respiration (ER)—has been studied across a range of spatial and temporal scales in recent decades to understand how climatic variability and disturbance regulate the regional-to-global carbon balance (Baldocchi, 2014; Braswell et al., 1997; Melillo et al., 2014; Yi et al., 2010). Environmental drivers, such as solar radiation, temperature, and air/soil moisture, are generally accepted as the major factors regulating the variation of CO_2 fluxes (i.e., F_{CO2}, GEP, ER) at the hourly to synoptic (multi-daily) scales (Baldocchi et al., 2001; Baldocchi, 2008; Stoy et al., 2005). On the other hand, the response of CO_2 fluxes to climatic variability becomes more complex at a longer scale (e.g., seasonal to interannual) and often involves indirect effects (i.e., prolonged, muted, and lagged responses) through altering the biotic characteristics (Barr et al., 2009; Humphreys and Lafleur, 2011; Richardson et al., 2010; Stoy et al., 2005). The interaction of direct and indirect effects is of great importance because the similarity or difference in their response magnitudes/directions to climatic variability may reveal the potential resilience or vulnerability of ecosystem carbon cycling to prospective climate change (Cox et al., 2000; Heimann and Reichstein, 2008; Luo et al., 2009).

Different statistical frameworks, such as the homogeneity-of-slopes model (e.g., Hui et al., 2003; McVeigh et al., 2014; Polley et al., 2008; Teklemariam et al., 2010) and the cross-year model simulation (e.g., Richardson et al., 2007; Shao et al., 2014; Wu et al., 2012), have been adopted to disentangle the direct/indirect effects. In general, these approaches took advantage of our current understanding of environmental forcing on the short-term variability of CO_2 fluxes. They structured the statistical models explicitly to incorporate all relevant short-term

4

70   environmental drivers (e.g., radiation, temperature, moisture) and allowed the model parameters

71   to vary across a longer time span (e.g., yearly, in most cases). Once the models were fitted, the

72   variation of CO_2 fluxes (e.g., among years) was then partitioned into the effects of environmental

73   drivers (i.e., direct effect) and model parameters (i.e., indirect effect). The changes of model

74   parameters were interpreted as "functional changes" (Hui et al., 2003), which comprised of all

75   effects that were unexplained by direct and instantaneous environmental forcing.

76   Potentially, the functional changes may result from the changes of plant phenology

77   (Richardson et al., 2009; Richardson et al., 2010), physiological characteristics (Luo et al., 2001;

78   Sala et al., 2010), canopy structure (Barr et al., 2004; Humphreys and Lafleur, 2011), soil

79   microbial community (Sowerby et al., 2005), substrate availability (DeForest et al., 2009), or the

80   interplay of autotrophic and heterotrophic respiration (DeForest et al., 2006; Xu et al., 2011).

81   Studies showed that the indirect effects often played a dominant role in driving interannual F_{CO_2}

82   variability (Shao et al., 2015). In some cases, the indirect effects explained up to ~70–80% of the

83   interannual variability of CO_2 fluxes (Shao et al., 2014; Wu et al., 2012). However, prior studies

84   have not been applied to a collection of co-located sites experiencing a set of extreme climate

85   anomalies, where the expectation would be similar responses given similar climate mean state

86   and geographic distance.

87   Recent research also highlighted the importance of rare but extreme weather events (e.g.,

88   heat/cold wave, rain storm, severe drought) for their disproportional influence on ecosystem

89   carbon cycling (Ciais et al., 2005; Shi et al., 2014; Wu et al., 2012; Xiao et al., 2010). Climatic

90   anomalies and extremes posed instantaneous effects on ecosystem carbon cycling by altering

91   environmental conditions (i.e., temperature, moisture). More importantly, these events may alter

92   the phenological, physiological, and structural traits of ecosystems, which then translate into

93   indirect effects that last much longer than the duration of climatic anomalies and extremes (Ciais

94   et al., 2005; Teklemariam et al., 2010; Thibault and Brown, 2008). These prolonged or lagged

95   effects often resulted in more influence on carbon cycling than the short-term direct effects

96   (Ciais et al., 2005; Desai, 2014; Thibault and Brown, 2008).

97   Most recently, severe weather and climate anomalies have been increasingly observed in

98   United States (Karl et al., 2012; Wuebbles et al., 2014). In the Great Lakes region, the recent

99   records included the earliest false spring of the century (2012), heat waves (2011, 2012), summer

100   cool spells (2013), and record-breaking high precipitation (2011) (Ault et al., 2013; Chu et al.,

101   2015; Karl et al., 2012). These anomalies triggered drastic year-to-year variation in plant

102   phenology across the region and caused severe damages to crop and fruit production (Ault et al.,

103   2013; Knudson, 2012). Our previous study found that a Lake Erie coastal marsh turned from a

104   net carbon sink to a net carbon source recently in the past years (Chu et al., 2015). However, it

105   remains unclear whether the influence was ecosystem-specific or region-wide, and to what extent

106   the influence was caused by direct and indirect effects.

107   Here, we aimed to examine and compare the effects of recent climatic variability and

108   anomalies on interannual variability of CO_2 fluxes at different ecosystems in the region.

109   Specifically, we targeted the two largest carbon fluxes (GEP and ER) and their balance—F_{CO2}.

110   We asked the following questions. (1) Do spatially co-located but functionally different

111   ecosystems respond similarly in magnitude and direction to climate variability and anomalies in

112   terms of CO_2 fluxes? (2) What biophysical factors most influence how ecosystem CO_2 fluxes

113   (GEP, ER, and F_{CO2}) respond to recent climate variability and anomalies? (3) To what extent can

114   the response of GEP, ER, and F_{CO2} be explained by the direct and indirect effects at different

115   ecosystems, respectively? Specifically, do these direct and indirect effects function

116 synergistically (++) or antagonistically (+−) to the climate variability and anomalies?

117

118 **2. Materials and Methods**

119 2.1. Experiment Design

120 We adopted a similar cross-year model simulation approach as in Richardson et al. (2007) and

121 Wu et al. (2012). We targeted the three most prevalent ecosystem types (i.e., agriculture, forest,

122 and wetland) in the study region—northwestern Ohio, USA. A Bayesian hierarchical model was

123 developed and the model parameters were estimated using the Markov Chain Monte Carlo

124 (MCMC) technique. The models were fitted against three-year (2011–2013) F_{CO2} data observed

125 at three eddy-covariance sites in the region (Table 1).

126 We designed the model to incorporate the most relevant short-term (hourly-synoptic)

127 environmental forcing on GEP and ER (i.e., solar radiation, temperature, air/soil moisture) and

128 allowed model parameters to vary through the seasons and over years. Once the models were

129 fitted, we ran a series of Monte Carlo simulations (N=1,000) at each half-hourly time step

130 through a yearly time span (17520 steps) by using model parameters from each year (2011–

131 2013) with environmental drivers from each year (2011–2013). The cross-year simulation

132 generated nine different scenarios of the parameter-driver combinations (e.g., 2011 driver × 2011

133 parameter, 2011 driver × 2012 parameter…). The simulated half-hourly GEP, ER, and F_{CO2} were

134 then integrated locally (i.e., every eight days) and annually.

135 Following Richardson et al. (2007), we adopted analysis of variance (ANOVA) to

136 partition the variation of local and annual integrals from the nine different simulation scenarios

137 into the effects of parameter years (i.e., indirect effect), driver years (i.e., direct effect), their

138 interactions (if significant), and residual errors. Instead of hypothesis testing, we adopted

139 ANOVA in order to interpret to what extent the simulated interannual GEP/ER/F_{CO2} variability

140 resulted from the instantaneous/direct response to the short-term environmental forcing. On the

141 other hand, interannual variability resulting from the varying parameters over the years was

142 interpreted as the lagged/prolonged response from altering the phenological, structural, or

143 physiological traits of ecosystems. Herein, we treated the nine scenario's composite average as a

144 conceptual baseline while presenting interannual variation of simulated GEP, ER and F_{CO2}.

145 Unless specified, we always reported parameter estimations and simulations in terms of medians

146 along with 95% quantile intervals (2.5%, 97.5%) in the following sections.

147

Table 1. Summary of the site location and vegetation types in the study.

Site	Oak Openings Preserve (US-Oho)	Curtice Walter-Berger Cropland (US-CRT)	Winous Point North Marsh (US-WPT)
Location	N41°33′16.98″ W83°50′36.76″	N41°37′42.31″ W83°20′43.18″	N41°27′51.28″ W82°59′45.02″
Vegetation type	Deciduous broadleaf forest (~70-year)	Conventional rain-fed cropland	Freshwater coastal marsh
Dominant species	*Quercus rubra*, *Q. alba*, *Q. velutina*, *Acer rubrum*	*Glycine max*, *Triticum spp.*	*Nymphaea odorata*, *Nelumbo lutea*, *Typha angustifolia*, *Hibiscus moscheutos*
Soil type	Sandy mixed and mesic	Silty clay	Hydric
Groundwater level	0.3–3 m belowground	0.3–3 m belowground	0.2–1 m aboveground
Soil water content	17–25%	25–65%	Saturated
Reference	Noormets et al. (2008b) Xie et al. (2014)	Chu et al. (2014)	Chu et al. (2014) Chu et al. (2015)

148

2.2. Site and Date Description

The three flux tower sites, which include a 70-year-old deciduous woodland in the Oak Openings Preserve (AmeriFlux: US-Oho), a freshwater marsh at the Winous Point Marsh Conservancy (US-WPT), and a conventional cropland (US-CRT) are located 30–50 km apart in northwestern Ohio (Table 1). The climate conditions are similar at the three sites with a long-term regional mean air temperature of ~10.0 °C and annual precipitation of ~897 mm (Chu et al., 2014). The mixed woodland is dominated by red oak (*Quercus rubra*), white oak (*Q. alba*), black oak (*Q. velutina*), and red maple (*Acer rubrum*). The freshwater marsh is permanently inundated and covered with a mix of narrow-leaved cattail (*Typha angustifolia*) and water lily (*Nymphaea odorata*) interspersed with areas of open water. The cropland site is rain-fed and no irrigation is applied. The cultivation practices include minimum tillage and both insect and weed control. During the three year study period, the cropland was planted with soybean (*Glycine max*) in 2011 (DOY 162–296) and 2012 (DOY 141–275). Winter wheat (*Triticum spp.*) was planted after the soybean harvest in 2012 and was harvested on DOY 197 in 2013. Detailed site information can be found in Chu et al. (2014; 2015), Noormets et al. (2008b), and Xie et al. (2014).

Micrometeorological variables were measured at all the sites, including photosynthetically active radiation (PAR), air temperature (T_a), vapor pressure deficit (VPD), precipitation (PP), soil temperature (T_g), groundwater level, and volumetric soil water content (VWC). Regional long-term meteorological data (i.e., T_a and PP) were obtained through the National Climatic Data Center of the National Oceanic and Atmospheric Administration, USA. The three-year (2011–2013) regional climate was summarized as being extremely warm in 2012 and having high precipitation in 2011 (Fig. A.1) (Chu et al., 2015). Additionally, there were several warm spells in 2011 and 2012 and cool spells in the summer of 2013.

172   The eddy covariance method was applied to quantify F_{CO_2} at all the sites following the

173   same workflow described in Chu et al. (2014). In total, 42%, 73% and 61% of F_{CO_2} passed the

174   quality control checks at the woodland, marsh, and cropland sites, respectively. The quality-

175   controlled and non-gap-filled F_{CO_2} was used for further model parameterization. In addition, we

176   applied the marginal distribution sampling (MDS) method to fill the F_{CO_2} gaps (Reichstein et al.,

177   2005). The MDS method was selected for its consistently good gap-filling performance across

178   sites (Moffat et al., 2007; Papale et al., 2006). Thus, we adopted the MDS-filled annual F_{CO_2} as a

179   reference estimate in comparison with those from the model simulations. Details of the gap-

180   filling procedures and uncertainty estimations can be found in our previous study (Chu et al.,

181   2014).

182   We adopted enhanced vegetation index (EVI) as a land surface vegetation index to

183   provide information of seasonal vegetation dynamics (e.g., canopy coverage, greenness, and

184   biomass) (Morisette et al., 2008). Eight-day EVI was calculated from the reflectance

185   (MOD09A1) of the Moderate Resolution Imaging Spectroradiometer (MODIS) instrument from

186   the Land Process Distributed Active Archive Center, US Geological Survey, USA. The target

187   spatial coverage was $500{\times}500$ m^2 at the marsh and cropland sites and $2{,}500{\times}2{,}500$ m^2 at the

188   woodland site, respectively.

189

190   2.3. Model Description

191   The F_{CO_2} was modeled at the half-hourly time step. We assumed F_{CO_2} followed a distribution,

192   where the mean (μ_{FCO_2}) can be modeled as the difference of GEP and ER. The standard deviation

193   (σ_{FCO_2}) can be modeled as a function of PAR to incorporate the heteroscedasticicity (Richardson

194   et al., 2006), where w_1 and w_2 were the empirical coefficients:

195 $$F_{CO2} \sim N(\mu_{FCO2}, \sigma_{FCO2}^2) \qquad (1)$$

196 $$\mu_{FCO2} = ER - I(PAR - 10) \cdot GEP; \quad I(x) = \begin{cases} 0, & x \le 0 \\ 1, & x > 0 \end{cases} \qquad (2)$$

197 $$\sigma_{FCO2} = w_1 + w_2 \cdot PAR; \quad w_i \sim N(\mu_{wi}, \sigma_{wi}^2) \qquad (3)$$

198 where the step function I(x) was used for discriminating the daytime/nighttime data (PAR>10

199 $\mu mol\ m^{-2}\ s^{-1}$ for daytime) such that the model could be estimated by using the daytime and

200 nighttime data together. Positive F_{CO2} indicated a net flux from the ecosystem to the atmosphere.

201 GEP and ER were both set to be positive.

202 The Arrhenius equation (Lloyd and Taylor, 1994) and Michaelis-Menten light response

203 equation (Falge et al., 2001) were adopted as the basic models for ER and GEP, respectively. In

204 addition, two exponential decaying functions were introduced to account for VPD limitation on

205 GEP and VWC limitation on ER (Lasslop et al., 2010; Noormets et al., 2008a):

206 $$ER = R_{ref} \cdot \exp\left[E_0\left(\frac{1}{T_{ref}-T_0} - \frac{1}{T_a-T_0}\right)\right] \cdot \varphi(VWC) \qquad (4)$$

207 $$GEP = A_{max} \cdot \left(\frac{PAR}{PAR+K_m}\right) \cdot \varphi(VPD) \qquad (5)$$

208 $$\varphi(VWC) = \begin{cases} 1, & VWC^* \ge VWC_0 \\ \exp[-k_{VWC}(VWC_0 - VWC^*)], & VWC^* < VWC_0 \end{cases} \qquad (6)$$

209 $$\varphi(VPD) = \begin{cases} 1, & VPD^* \le VPD_0 \\ \exp[-k_{VPD}(VPD^* - VPD_0)], & VPD^* > VPD_0 \end{cases} \qquad (7)$$

210 where VPD^* and VWC^* were the normalized VPD (0–1) and VWC (0–1) against the observed

211 full ranges. R_{ref} ($\mu mol\ CO_2\ m^{-2}\ s^{-1}$) was the base respiration at the reference temperature (T_{ref}, set

212 as 10°C), E_0 (°C) was the temperature sensitivity, T_0 was set to be −46.02°C, A_{max} ($\mu mol\ CO_2\ m^{-2}\ s^{-1}$)

213 s^{-1}) was the maximum ecosystem CO_2 uptake rate at light saturation, and K_m ($\mu mol\ quanta\ m^{-2}$

214 s^{-1}) was the half-saturation quantum flux level of the GEP light response curve. k_{VPD} and k_{VWC}

215 represented the sensitivities for VPD and VWC limitation whereas VPD_0 and VWC_0 were the

216   thresholds for VPD and VWC limitation.

217   In the preliminary tests, we found that certain parameters (e.g., A_{max}-K_m-k_{VPD}-VPD_0)

218   tended to co-vary. If all these parameters were allowed to vary through the time series without

219   proper constraints, model parameterization either did not converge or led to unreasonable

220   estimations when it did. Thus, we reduced the model structures based on current knowledge

221   about these parameters' temporal characteristics and set different parameters to vary at specific

222   time steps (Appendix A) (Bloom and Williams, 2015; Shao et al., 2014). R_{ref} and A_{max} were

223   allowed to vary every day within each year and among years while the rest (e.g., E_0, K_m…) were

224   set to only vary among years (i.e., yearly parameter). Furthermore, we adopted the phenology

225   model in Gu et al. (2009) to describe the seasonal dynamics of R_{ref} and A_{max}, where R_{ref} and A_{max}

226   at each daily step were modeled as functions of the day of year (DOY) (i.e., $\mu_{Amax}(t)$, $\mu_{Rref}(t)$).

227   Additionally, the standard deviations (i.e., σ_{Amax}, σ_{Rref}) were introduced so that R_{ref} and A_{max} can

228   be fine-tuned at each daily step to mimic the multi-day variation that superimposed the

229   seasonality:

230    $$R_{ref}(t) \sim N(\mu_{Rref}(t), \sigma_{Rref}^2) \tag{8}$$

231    $$A_{max}(t) \sim N(\mu_{Amax}(t), \sigma_{Amax}^2) \tag{9}$$

232    $$\mu_x(t) = y_{0.x} + \frac{a_{1.x}}{\left[1+\exp\left(-\frac{t-t_{1.x}}{b_{1.x}}\right)\right]^{c_{1.x}}} - \frac{a_{2.x}}{\left[1+\exp\left(-\frac{t-t_{2.x}}{b_{2.x}}\right)\right]^{c_{2.x}}} \tag{10}$$

233   where t represented the DOY, the first term (y_0) on the right hand side of Eq. (10) represented the

234   baseline R_{ref} or A_{max} of the year and the second and third terms reflected the spring development

235   and fall recession phases of R_{ref} or A_{max}. y_0, a_1, a_2, b_1, b_2, c_1, c_2, t_1, and t_2 were empirical

236   parameters that were associated with either the full ranges of R_{ref} or A_{max} (y_0, a_1, a_2) or the

237   duration/timing of the transition periods (b_1, b_2, c_1, c_2, t_1, t_2). Once the models were fitted, a

238   series of ensemble phenological characteristics, such as the annual assimilation/respiration

239   potentials (i.e., annual integrals), active and peak assimilation/respiration periods, can be

240   calculated from the model coefficients (Table A.1; Appendix A) (Gu et al., 2009). While fitting

241   the models, we set all the empirical parameters in Eq. (10) to vary among years in representing

242   the interannual variation.

243   In our preliminary tests, we also found that the yearly estimates of k_{VWC}, VWC_0, k_{VPD},

244   and VPD_0 were similar among years. Thus, we further reduced the model structures by treating

245   them as universal parameters (i.e., one set of parameters for three years) similar to other previous

246   studies (e.g., Richardson et al., 2007; Shao et al., 2014). For each yearly parameter, we assumed

247   that the parameters were linked among years (i.e., exchangeability) and the linkage could be

248   described by a higher level distribution (i.e., hierarchical model):

249           $\theta_{jl} \sim N(\mu_{\theta j}, \sigma_{\theta j}^2); \ \theta_{jl} \in [L_{\theta j}, U_{\theta j}]$ (11)

250   where θ_{jl} was a yearly estimate of parameter θ_j (e.g., E_0, K_m, y_0, a_1, a_2, b_1, b_2…) at the year l

251   (2011–2013), $\mu_{\theta j}$ and $\sigma_{\theta j}$ were the mean and standard deviation of the higher level distribution

252   from which θ_{jl} was drawn (i.e., hyper parameters). A uniform prior was adopted for each hyper

253   parameter (i.e., $\mu_{\theta j}$, $\sigma_{\theta j}$) bounded within an acceptable range based on literature survey (Table 2;

254   Table A.2; Table A.3; Table A.4) (Zobitz et al., 2011). Also, each yearly parameter was

255   constrained by the lower ($L_{\theta j}$) and upper ($U_{\theta j}$) bounds.

256   While fitting the model, we estimated all the parameters in Eqs. (1)–(11) together with

257   the entire three-year dataset. For the cropland site, the winter-spring wheat cover at the cropland

258   had two higher assimilation periods (October–November 2012 and May–June 2013) that were

259   separated by the snow-covered period in winter. Thus, an additional set of model parameters was

260   introduced specifically for this winter-wheat period (September–December 2012) in order to

261   adequately capture the bimodal seasonality of A_{max} in 2012.

13

262   The GEP and ER models are admittedly semi-empirical. However, as the models were

263   fine-tuned to incorporate the major short-term environmental drivers (e.g., PAR/VPD on GEP,

264   T_a/VWC on ER) of these ecosystems (Chu et al., 2014; Noormets et al., 2008b; Ouyang et al.,

265   2014), the A_{max} and R_{ref} represented the potential GEP and baseline ER after eliminating the

266   short-term dynamics of environmental forcing. We did not use site-specific management factors

267   (e.g., agricultural practice at the cropland, groundwater level at the marsh) in order to keep the

268   model structures and thus variance partition comparable among sites. Herein, these parameters

269   were interpreted as estimates of ecosystem functional traits that were associated with GEP and

270   ER (i.e., functional parameter) (Wu et al., 2012). For example, A_{max} was addressed to be often

271   associated with ecosystem structural (e.g., leaf area index) and physiological (e.g., leaf

272   photosynthesis capacity, nitrogen content) characteristics (Cook et al., 2004; Ollinger et al.,

273   2008). R_{ref} was often associated with the substrate quality/quantity and microbial

274   composition/activity (Carbone et al., 2008; Cook et al., 2004; Jarvis et al., 2007).

275

276   2.4. Model Parameterization and Model Error Assessment

277   All statistical tests and model estimations were conducted in the R platform (R Development

278   Core Team, 2014, version 3.1.1). Bayesian hierarchical models were carried out using the JAGS

279   software (Just Another Gibbs Sampler, version 3.4.0) (Plummer, 2003), which was activated

280   through the "rjags" package. The "dclone" and "snow" packages were used for parallel

281   computation of six chains starting randomly within the prior ranges (Solymos, 2010; Tierney et

282   al., 2009). The Gelman-Rubin convergence was checked by using the "coda" package (Brooks

283   and Gelman, 1998; Plummer et al., 2006). The chains usually converged after less than 15,000–

284   17,000 iterations. After convergence, we ran an updating stage of 5,000 iterations, and a final

285   burn-in stage of 3,000 iterations. Finally, we kept 1,000 parameter sets for following simulations

286   by thinning the last 3,000 iterations from all of the six chains (i.e., 167 per chain) to eliminate the

287   autocorrelation of estimates among iterations.

288   Once the models were fitted, we examined the model performance via a series of inter-

289   comparison between the predicted F_{CO2} ($F_{CO2.model}$) and observed/gap-filled F_{CO2}

290   ($F_{CO2.obs}$/$F_{CO2.fill}$). First, we used a simple linear regression to compare the half-hourly $F_{CO2.model}$

291   against $F_{CO2.obs}$ for each year. The comparison was also done for the daily and eight-day $F_{CO2.model}$

292   against $F_{CO2.fill}$ for each year. The temporal scales were selected to target the two dominant

293   characteristic scales in the F_{CO2} time series (i.e., daily–synoptic and seasonal–annual scales)

294   (Baldocchi et al., 2001; Desai, 2010; Ouyang et al., 2014). The comparison of $F_{CO2.model}$ and

295    $F_{CO2.fill}$ was made only for those periods that had less than 50% of gap-filled data. The model

296   error statistics provided an estimate of the unexplained variation by our models, which resulted

297   from the uncertainties both in the EC measurements and model parameterization. Second, we

298   examined the agreement between $F_{CO2.model}$ and $F_{CO2.fill}$ at different times and timescales via

299   wavelet coherence (Grinsted et al., 2004; Stoy et al., 2013). The "biwavelet" package was

300   adopted to calculate the wavelet coherence across a wide range of scales (2^0–2^{13} hours) (Gouhier,

301   2014). Following Grinsted et al. (2004), we interpreted the coherence as an estimate of

302   correlation between two time series across times and timescales and the coherence threshold was

303   set as 0.7 for determining the significance (i.e., >0.7 as significant coherence).

304

305   **3. Results**

306   3.1. Model Diagnostics and Error Statistics

307   The modeled F_{CO2} showed significant wavelet coherence against the observed F_{CO2} at the half-

308   daily to daily scale (~2^3–2^5 hours) during the growing season and at the annual scale (~2^{12}–2^{13}

309   hours) through the study period at all the sites (Fig. 1). There was a longer data gap (~16 days) at

310   the marsh site in the 2012 fall, during which the modeled F_{CO2} deviated unmistakably from the

311   MDS-filled F_{CO2} (Fig. 1c). Outside this long-gap event, the simulated F_{CO2} showed significant

312   wavelet coherence against the observed F_{CO2} at the multi-daily to monthly scales (~2^7–2^{10} hours)

313   at all the sites. The inter-comparison of observed/gap-filled and modeled F_{CO2} had slopes ranging

314   between 1.00–1.03, 0.99–1.05, and 0.97–1.08 at the half-hourly, daily, and eight-day scales

315   (Table A.5), suggesting that the model was generally robust and unbiased in duplicating the F_{CO2}

316   variability across the target scales at all sites.

317   The simulated F_{CO2} generally replicated the interannual variability that was compatible

318   with the gap-filled F_{CO2} at all sites (Fig. A.2). Noticeably, the simulated annual F_{CO2} deviated

319   from the gap-filled annual F_{CO2} in terms of the absolute magnitudes. For the woodland and

320   cropland sites, the net annual CO_2 uptake was consistently higher from model simulation than

321   gap-filling (~22% and ~11%, respectively). We found the difference of cumulative F_{CO2} occurred

322   mostly in the non-growing seasons and was generally negligible in the growing seasons (Fig. 1;

323   Fig. A.2). The deviations resulted mostly from a few high F_{CO2} pulse events that were likely

324   associated with intermittent nighttime turbulence, CO_2 outbursts after snow meltdown/ice

325   breakup, or pulsing CO_2 release after rainfalls (at the marsh). As our current model was not

326   designed to incorporate these intermittent events (either drivers or model structures), our model

327   failed to reproduce these pulsing patterns and thus led to underestimation of cumulative F_{CO2} in

328   the non-growing seasons. However, our model simulation still succeeded in replicating the

329   interannual variability of the annual F_{CO2}, which was largely determined by the interannual

330   variability of growing season F_{CO2}. Thus, we argued that the model framework was suitable and

331   robust for our current research purpose. The standard deviations of annual F_{CO2} were compatible

16

332   between the gap-filled and simulated data, ranging between 51–61, 79–84, and 86–87 g C m^{-2}

333   yr^{-1} at the woodland, cropland, and marsh sites, respectively.
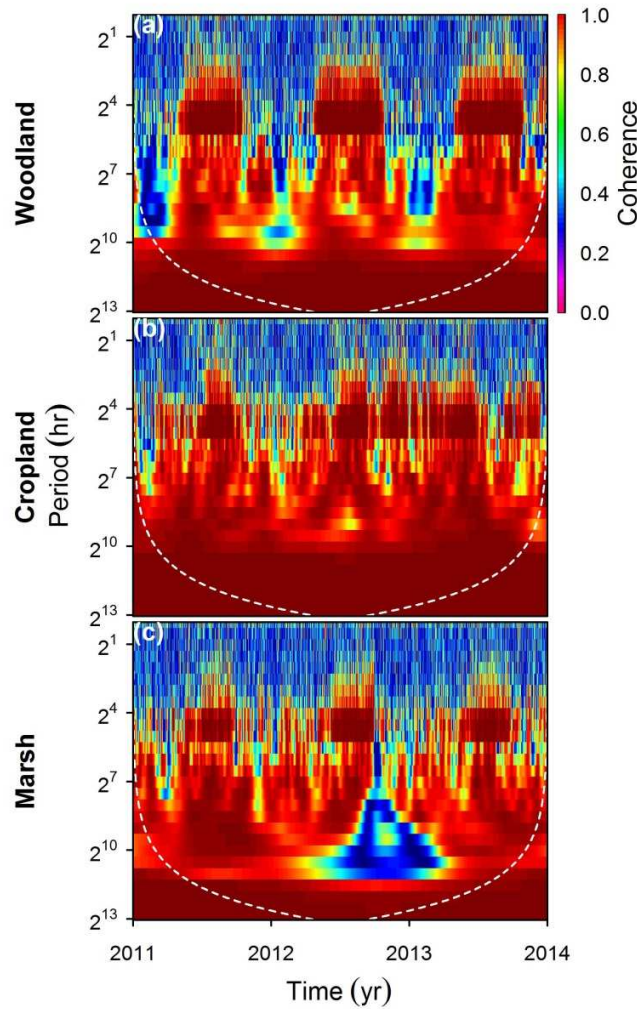
334

335   **Fig. 1.** Wavelet coherence between the observed (gap-filled) and modeled net ecosystem CO_2
336   exchanges (F_{CO2}) along the time and timescale (period) axes. The colorbar denotes the wavelet
337   coherence and the coherence threshold is set as 0.7 for determining the significance (i.e., >0.7 as
338   significant coherence). The dashed lines indicate the cones of influence beyond which the
339   wavelet coherence should not be interpreted. (For interpretation of the references to color in this
340   figure legend, the reader is referred to the web version of the article.)

17

3.2. Functional Parameters

Our models adequately mimicked the multi-scaled nature (multi-daily, seasonal, and interannual variability) of our target functional parameters—R_{ref} and A_{max} (Fig. 2; Fig. 3). That allowed us to detect the interannual difference of ensemble phonological characteristics, such as the annual integrals and timing of active/peak growing periods (Fig. 2a, c, e; Fig. 3a, c, e; Fig. A.3), while still preserving the information of short-term dynamics (Fig. 2b, d, f; Fig. 3b, d, f). The estimated A_{max} and R_{ref} were significantly correlated with EVI (Cor: 0.62–0.97) (Fig. A.4), suggesting that their seasonal dynamics were largely associated with the ecosystem vegetation greenness.

At the woodland site, the warm year of 2012 had the longest peak assimilation periods of 125 days whereas 2011 and 2013 had 90 and 103 days, respectively, and led to the highest annual assimilation potential among the three years (Fig. 2a; Fig. A.3). The earlier onset of the assimilation period in 2012 was largely associated with higher soil temperature (Fig. A.4a). At the marsh site, the seasonal dynamics of A_{max} varied only marginally between 2011 and 2012 (Fig. 2e; Fig. A.3a, c). The shortest duration of assimilation period (5–13 days shorter) and the lowest annual assimilation potential (29–33% lower) at the marsh were observed in 2013 (Fig. A.3a, c). The cool summer of 2013 led to the lowest peak A_{max} (~20 μmol m^{-2} s^{-1}) and the senescence period started around 11–16 days earlier than in 2011 and 2012 (Fig. 2e; Fig. A.3c). Noticeably, the dependence of A_{max} on soil temperature in 2013 deviated from that in 2011 and 2012 (Fig. A.4i), suggesting that the early fall senescence in 2013 was influenced by other factors (e.g., chilling damage).

As expected, A_{max} at the cropland site varied greatly over the years (Fig. 2c, d) and the recovery and senescence of A_{max} did not follow closely with soil temperature (Fig. A.4e). This suggested that the GEP phenology was largely influenced by agricultural management, such as

364 crop types and plantation/harvest schedules. Considering only the periods with soybean cover,

365 the peak A_{max}, assimilation potentials and duration of active and peak assimilation periods varied

366 only marginally between 2011 and 2012 (Fig. 2c; Fig. A.3a, c).

367   The ensemble characteristics of ER phenology, such as the peak R_{ref} and length of the

368 active and peak respiration periods, also varied markedly over the years (Fig. 3; Fig. A.3b, d).

369 The duration of peak respiration periods generally coincided with the peak assimilation periods

370 at each site (Fig. A.3c, d). This suggested that GEP and ER phenology were generally

371 synchronized in time. As expected, the woodland site had the longest active/peak respiration

372 periods and the highest annual respiration potential in 2012. To our surprise, the annual

373 respiration potential was not significantly higher in 2012 at the cropland site. Also, the annual

374 respiration potential was not significantly lower in 2013 at the marsh site. As such, the

375 magnitudes of GEP and ER phenology (e.g., annual potentials, peak values) may not change

376 consistently nor respond evenly to interannual climatic variability.

377   Yearly parameters (i.e., E_0, K_m) also varied slightly between years (Table 2). However,

378 the difference needs to be interpreted with care. As stated earlier, these parameters tended to co-

379 vary with A_{max} or R_{ref}. Therefore, treating them as separate and independent estimates may risk

380 over-interpretation. For example, different E_0 was estimated among years at all the sites. This

381 interannual difference, however, coincided with the interannual difference of peak R_{ref} (Fig. 3;

382 Table 2). Hereafter, we treat parameters obtained from each year and each model as a set that

383 represented the comprehensive functional status of GEP or ER for each year (e.g., 2011

384 parameter). The parameters from each year were used together running the cross-year model

385 simulation and the effects of different environmental drivers in each year were not further

386 partitioned in the study.

19

387
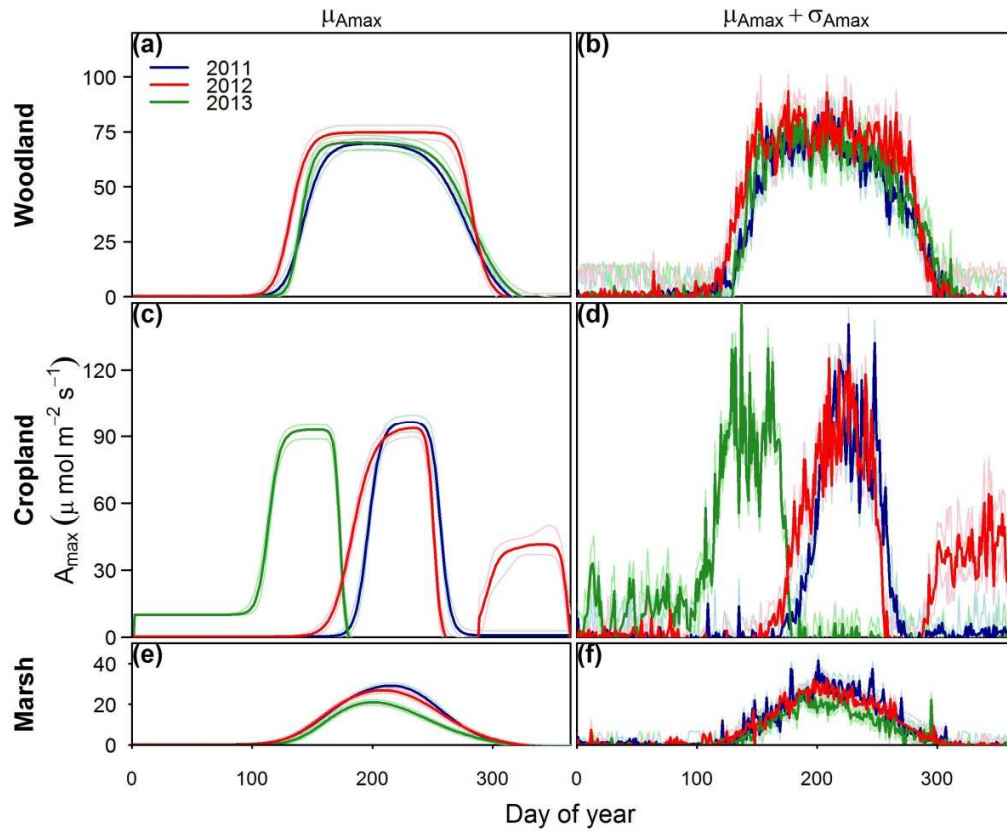
Fig. 2. Time series of the daily maximum ecosystem CO_2 uptake rate at light saturation (A_{max}), including (a, c, e) the mean estimates (μ_{Amax}) and (b, d, f) the means with random errors ($\mu_{Amax}+\sigma_{Amax}$). Light colored lines represent the 95% posterior quantile intervals. (For interpretation of the references to color in this figure legend, the reader is referred to the web version of the article.)

20

393
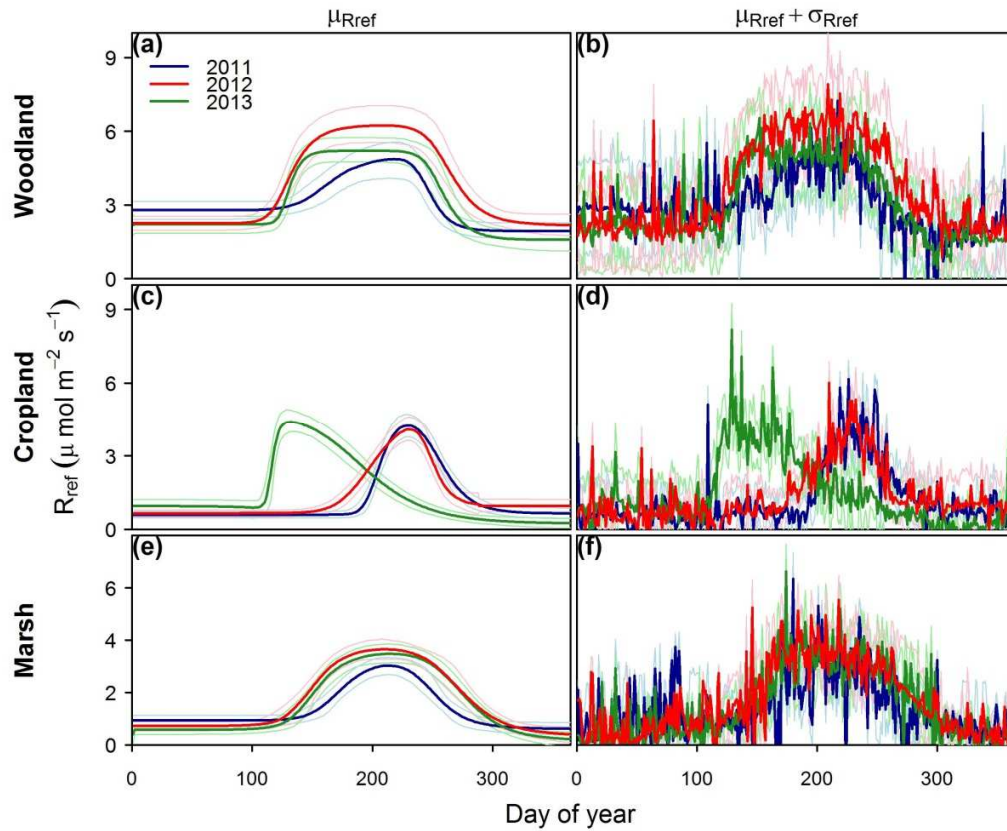
Fig. 3. Time series of the daily reference respiration (R_{ref}), including (a, c, e) the mean estimates
(μ_{Rref}) and (b, d, f) the means with random errors ($\mu_{Rref}+\sigma_{rref}$). Light-colored lines represent the
95% posterior quantile intervals. (For interpretation of the references to color in this figure
legend, the reader is referred to the web version of the article.)

Table 2. Medians and 95% quantile intervals (2.5%, 97.5%) of the posterior distributions and the lower and upper bounds [lower, upper] of the uniform prior distributions of model parameters at the woodland, marsh, and cropland sites[a]

Parameter	Posterior			Prior
	2011	2012	2013	Hyper parameter
Woodland site				
E_0	232 (232,261)	58 (50,77)	52 (50,58)	[50,400]
K_m	1330 (1237,1424)	1762 (1644,1896)	1822 (1666,1968)	[100,2000]
k_{VWC}		0.67 (0.46,0.88)		[0,10]
VWC_0		0.55 (0.47,0.63)		[0,10]
k_{VPD}		0.82 (0.77,0.87)		[0,10]
VPD_0		0.18 (0.17,0.20)		[0,10]
Marsh site				
E_0	178 (160,196)	86 (68,105)	91 (71,109)	[50,400]
K_m	662 (607,718)	690 (619,760)	430 (383,483)	[100,2000]
k_{VWC}		n.a.		[0,10]
VWC_0		n.a.		[0,10]
k_{VPD}		0.42 (0.15,0.76)		[0,10]
VPD_0		0.45 (0.23,0.53)		[0,10]
Cropland site				
E_0	205 (181,229)	186 (162,210)	76 (55,102)[b]	[50,400]
K_m	1316 (1237,1391)	1184 (1111,1246)	1533 (1459,1612)[b]	[100,2000]
k_{VWC}	0.78 (0.09,8.30)		0.91 (0.29,8.63)[b]	[0,10]
VWC_0	0.32 (0.01,0.74)		0.76 (0.04,0.92)[b]	[0,10]
k_{VPD}	1.23 (1.17,1.29)		0.89 (0.79,0.98)[b]	[0,10]
VPD_0	0.09 (0.07,0.10)		0.06 (0.03,0.07)[b]	[0,10]

[a]E_0: temperature sensitivity (°C); K_m: half-saturation quantum flux level of the GEP light response curve (μmol quanta m^{-2} s^{-1}); k_{VPD}: sensitivity for vapor pressure deficit (VPD) limitation; k_{VWC}: sensitivity for soil water content (VWC) limitation; VPD_0: threshold for VPD limitation; VWC_0: thresholds for VWC limitation; n.a.: not available.
[b]For wheat period (September 2012–2013).

398

399 3.3. Direct and Indirect Effects on Variability of Local Eight-Day GEP, ER, and F_{CO2}

400 Both direct and indirect effects explained a substantial portion of the local eight-day variation of

401 GEP, ER, and F_{CO2} over the years (Fig. 4; Fig. 5; Fig. 6). Additionally, their relative contribution

402 (either in direction or in magnitude) varied substantially through time and among sites. Briefly,

403 the local variability of GEP, ER, and F_{CO2} at the cropland was dominantly driven by the indirect

404 effects (Fig. 4), reflecting largely the year-to-year difference in the crop plantation and harvest

22

405　schedules. The growing periods at the cropland site were relatively short, where A_{max} and R_{ref}

406　varied drastically and rapidly. Thus, any change in the planting schedule and/or crop types

407　produced a substantial difference in the local eight-day GEP, ER, and F_{CO2} over the years (up to

408　±80, ±30, and ±60 g C m^{-2} 8d^{-1}). Woodland and marsh sites, in contrast, had relatively smaller

409　local eight-day variability over the years that was generally bounded within ±20 and ±15 g C m^{-2}

410　8d^{-1} (Fig. 5; Fig. 6).

411　　　The warm spells in spring and summer in 2011 and 2012 affected the local variability of

412　GEP, ER, and F_{CO2} mainly through the indirect effects that triggered the shifts of growing periods

413　over the years (Fig. 4; Fig. 5; Fig. 6; Fig. A.1). There were direct effects on ER that were caused

414　by warm air temperature, but the effects were marginal and generally less than ~10 g C m^{-2} 8d^{-1}

415　at all the sites. The woodland site had ~70 and ~30 g C m^{-2} higher GEP modulated by the

416　indirect effect in the early and late growing periods (DOY 121–153 and 257–281) in 2012 (Fig.

417　5a). On the other hand, the relatively drier atmosphere (higher VPD) in the late summer (DOY

418　217–241) in 2012 led to ~28 g C m^{-2} lower GEP through the direct effect (Fig. 5a; Fig. A.1c). As

419　ER was only slightly higher in the growing period in 2012 (~6 g C m^{-2}), the net CO_2 uptake

420　increased ~81 g C m^{-2} at the woodland site (Fig. 5c). Similarly, the marsh site had marginally

421　higher GEP in 2012 as a consequence of indirect effects (Fig. 6a). As GEP was less limited by

422　the dry atmosphere at the marsh site than the woodland site, the direct effect, in contrast,

423　enhanced the marsh GEP as a result of higher PAR in the relatively rainless summer of 2012

424　(Fig. 6a; Fig. A.1a, b, c). In total, the marsh site had ~48 and ~22 g C m^{-2} higher GEP caused by

425　the direct and indirect effects in the growing period of 2012. In contrast to the woodland site, the

426　marsh site had higher ER in the growing period of 2012 mostly resulting from the indirect effect

427　(~25 g C m^{-2}). Consequently, the net CO_2 uptake increased by ~29 g C m^{-2} at the marsh site in
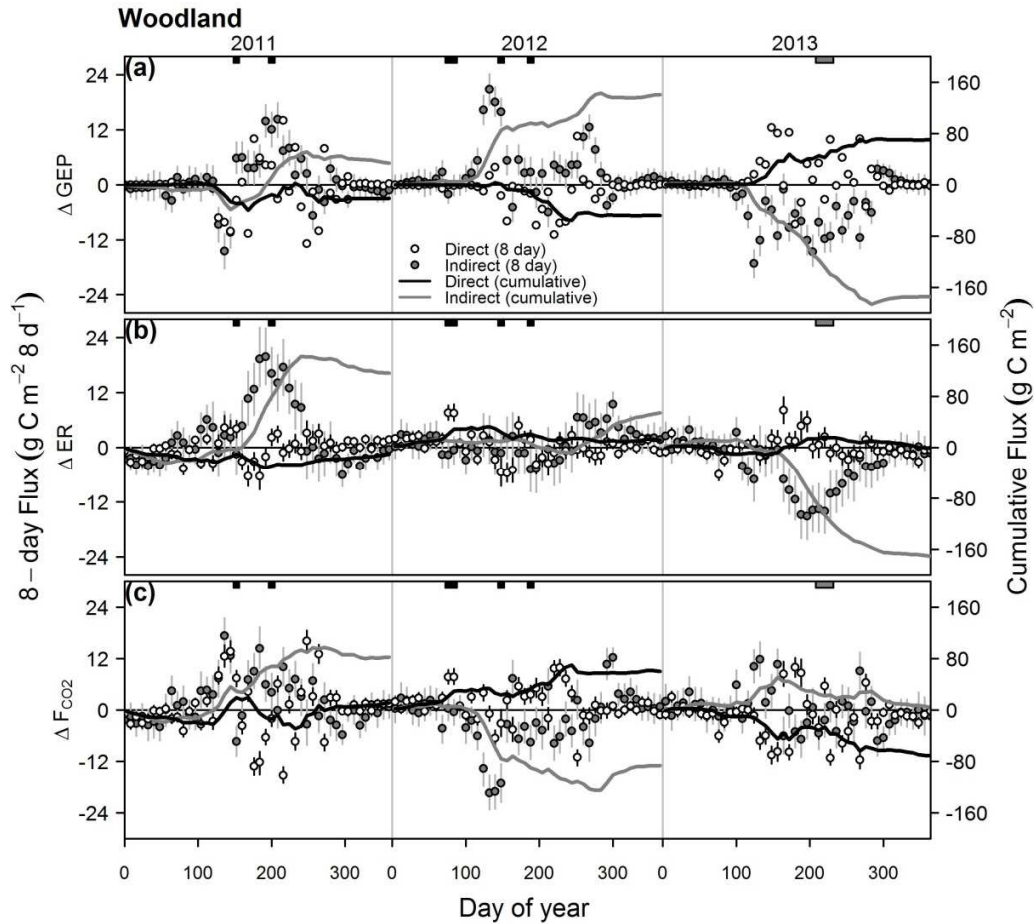
428   the growing period of 2012 (Fig. 6c).

429   The late summer cool spells of 2013 (DOY 208-239) posed a substantial and opposite

430   effect on CO_2 fluxes at the woodland and marsh sites (Fig. 5; Fig. 6). At the woodland site, the

431   32-day cumulative CO_2 uptake was ~17 g C m^{-2} higher in 2013 than the three-year average (Fig.

432   5c). The enhanced CO_2 uptake was largely attributed to lower ER (~38 g C m^{-2}) modulated by

433   the indirect effects (Fig. 5b). The indirect and direct effects on GEP compensated each other to a

434   large extent and led to only a ~20 g C m^{-2} decrease in GEP. The marsh site, in contrast, had a

435   lower net CO_2 uptake during the cool summer period of 2013 of ~11 g C m^{-2} below the three-

436   year average (Fig. 6a). Remarkably, the reduction of CO_2 uptake lasted much longer than the

437   duration of the cool event until the end of growing period (~DOY 272). In total, the net CO_2

438   uptake was ~42 g C m^{-2} lower from DOY 240 to the end of growing period in 2013 in

439   comparison with the three-year average. This lower CO_2 uptake was dominantly driven by the

440   indirect effect on GEP (~51 g C m^{-2}, Fig. 6c) while ER was generally compatible comparing to
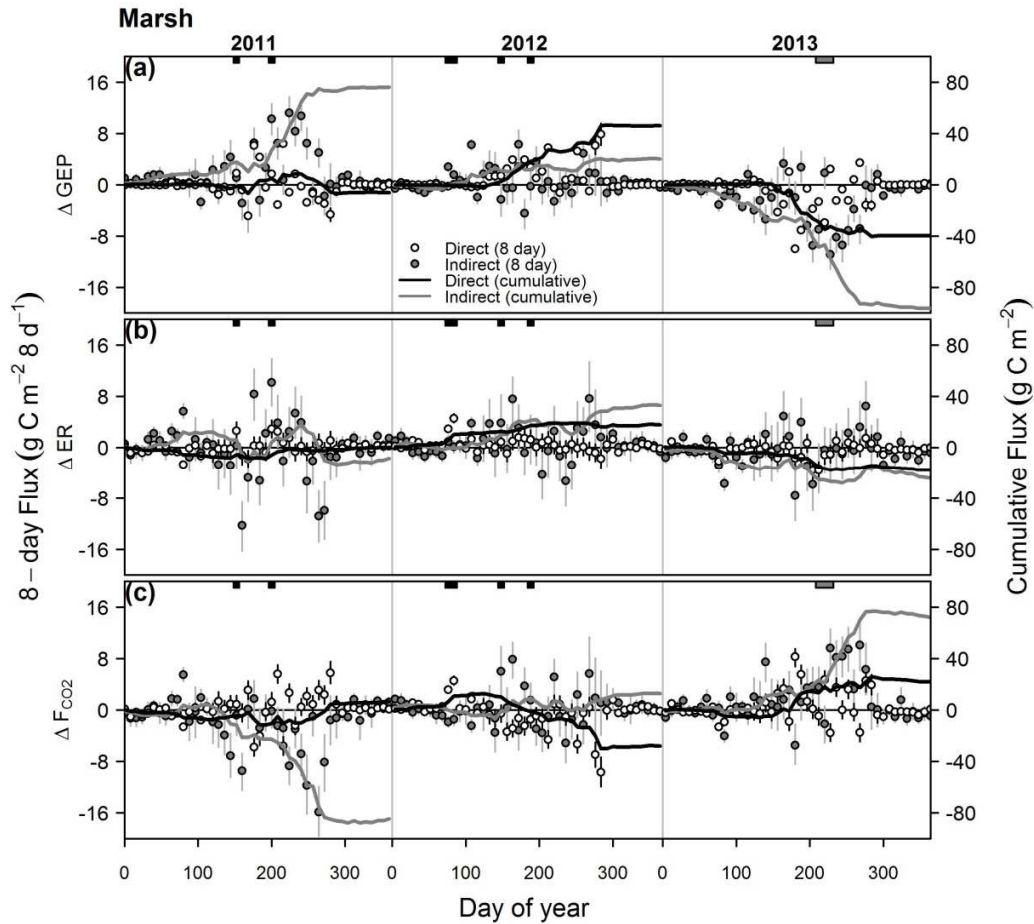
441   2011 and 2012.
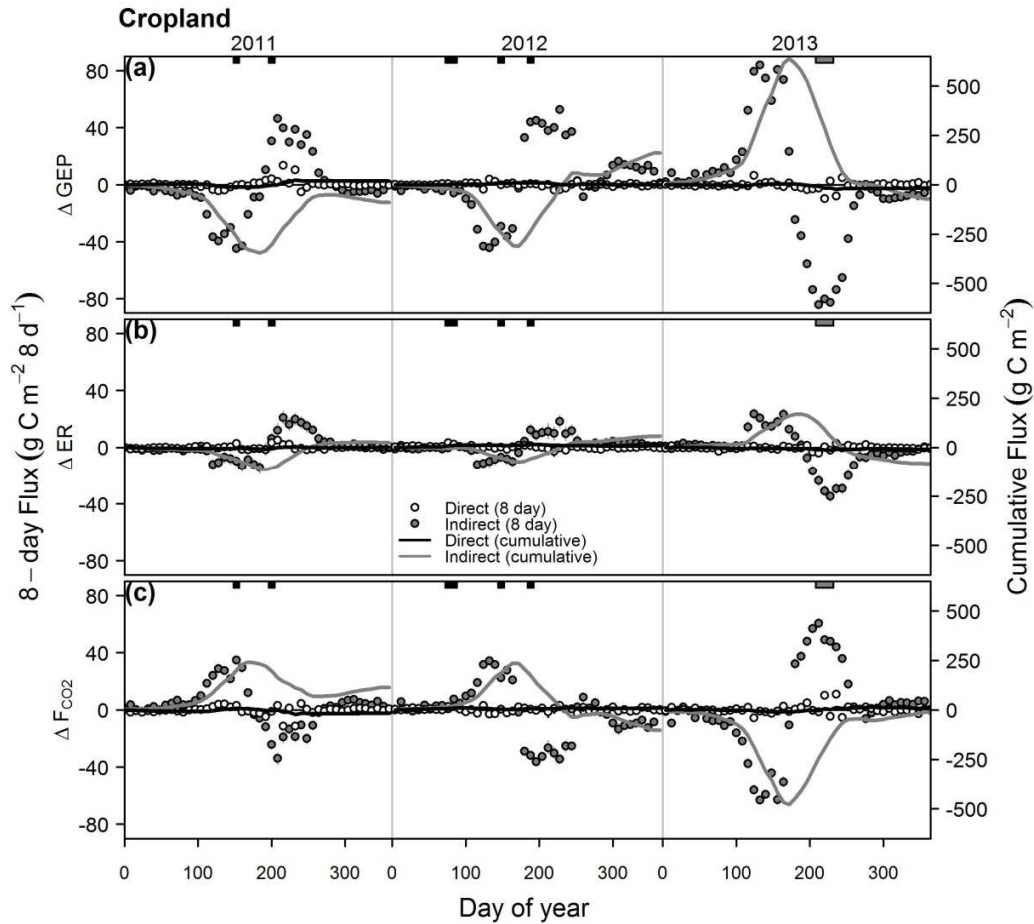
Fig. 4. The effects of year-to-year variation in environmental drivers and model parameters on modeled (a) gross ecosystem production (ΔGEP), (b) ecosystem respiration (ΔER), and (c) net ecosystem CO_2 exchange (ΔF$_{CO2}$) at the cropland site. Variation of each eight-day integrated fluxes over the years was partitioned into effects of environmental drivers (direct effect) and model parameters (indirect effect). The baseline (i.e., 0) was set as the average of nine-scenario simulations in each eight-day period. The sign convention is that a positive effect on ER and GEP increases the respiration loss and assimilation uptake whereas a negative effect on F$_{CO2}$ increases the net ecosystem CO_2 uptake. Cumulative effects were calculated starting from the first day of each year. Vertical segments indicate the 95% quantile intervals of model simulation. Black and grey blocks indicate the duration of climate anomaly events (warm and cool spells) similar to Fig. A.1a.

454

Fig. 5. The effects of year-to-year variation in environmental drivers and model parameters on modeled (a) gross ecosystem production (ΔGEP), (b) ecosystem respiration (ΔER), and (c) net ecosystem CO_2 exchange (ΔF_{CO2}) at the woodland site. Variation of each eight-day integrated fluxes over the years was partitioned into effects of environmental drivers (direct effect) and model parameters (indirect effect). The baseline (i.e., 0) was set as the average of nine-scenario simulations in each eight-day period. The sign convention is that a positive effect on ER and GEP increases the respiration loss and assimilation uptake whereas a negative effect on F_{CO2} increases the net ecosystem CO_2 uptake. Cumulative effects were calculated starting from the first day of each year. Vertical segments indicate the 95% quantile intervals of model simulation. Black and grey blocks indicate the duration of climate anomaly events (warm and cool spells) similar to Fig. A.1a.

466

Fig. 6. The effects of year-to-year variation in environmental drivers and model parameters on modeled (a) gross ecosystem production (ΔGEP), (b) ecosystem respiration (ΔER), and (c) net ecosystem CO_2 exchange (ΔF_{CO2}) at the marsh site. Variation of each eight-day integrated fluxes over the years was partitioned into effects of environmental drivers (direct effect) and model parameters (indirect effect). The baseline (i.e., 0) was set as the average of nine-scenario simulations in each eight-day period. The sign convention is that a positive effect on ER and GEP increases the respiration loss and assimilation uptake whereas a negative effect on F_{CO2} increases the net ecosystem CO_2 uptake. Cumulative effects were calculated starting from the first day of each year. Vertical segments indicate the 95% quantile intervals of model simulation. Black and grey blocks indicate the duration of climate anomaly events (warm and cool spells) similar to Fig. A.1a.

27

478 3.4. Direct and Indirect Effects on Variability of Annual GEP, ER, and F_{CO2}

479 Indirect effects generally explained a substantial portion of the interannual variability in annual

480 GEP, ER, and F_{CO2} at all the sites (Fig. 7). However, the relative contribution of direct and

481 indirect effects varied among different CO_2 fluxes and sites. Noticeably, a large portion of the

482 local eight-day variability at the cropland was compensated over time while integrating into

483 annual integrals (Fig. 4; Fig. 7c). Despite the absolute magnitudes of annual F_{CO2} differed

484 evidently from around −500 and −300 g C m^{-2} yr^{-1} at the woodland and cropland to near 0 g C

485 m^{-2} yr^{-1} at the marsh, the interannual variability was surprisingly compatible and within 61–86

486 (SD) g C m^{-2} yr^{-1} at all the sites (Fig. 7a, c, e).

487 The interannual variation of annual F_{CO2} was mainly driven by the varying parameters

488 over the years, accounting for 54%, 89%, and 86% of the variation at the woodland, cropland,

489 and marsh sites, respectively. Such indirect effects translated to ±85, ±110, and ±85 g C m^{-2} yr^{-1}

490 year-to-year difference in the annual F_{CO2} (Fig. 7b, d, f). On the other hand, the varying climate

491 conditions over the years accounted for 33% of the interannual F_{CO2} variation at the woodland

492 site and became irrelevant (<10%) at the cropland and marsh sites. Such direct effects led to ±70,

493 ±16, and ±28 g C m^{-2} yr^{-1} year-to-year difference in the annual F_{CO2} at the woodland, cropland,

494 and marsh sites, respectively. At all the sites, the interannual variation of GEP was dominantly

495 driven by indirect effects, which accounted for 79–91% of interannual variation (i.e., ±96–±175

496 g C m^{-2} yr^{-1} year-to-year difference). For ER, indirect effects dominated the interannual

497 variation at the woodland and cropland sites (91% and 90%) while accounting for only 51% of

498 the interannual variation at the marsh site.

499 The indirect effects on annual GEP and ER generally varied in the same directions over

500 the years (Fig. 7b, d, f; Fig. A.5e; Cor: 0.72). That means, the increase of annual GEP induced by

indirect effects was usually accompanied by the increase of annual ER also induced by indirect effects. We did not find similar co-varying patterns in the direct effects on annual GEP and ER, or between the direct and indirect effects on all fluxes (Fig. A5b, c, d, f; Cor: −0.45-0.35). In sum, GEP and ER—the two large and opposite fluxes that determine the annual net CO_2 uptake, tend to co-vary over the years and sites. Such co-varying pattern is mostly driven by the synchronous changes (in directions) of indirect effects on GEP and ER. Consequently, the interannual variability of annual F_{CO2} is surprisingly conservative and compatible among all the sites.

509
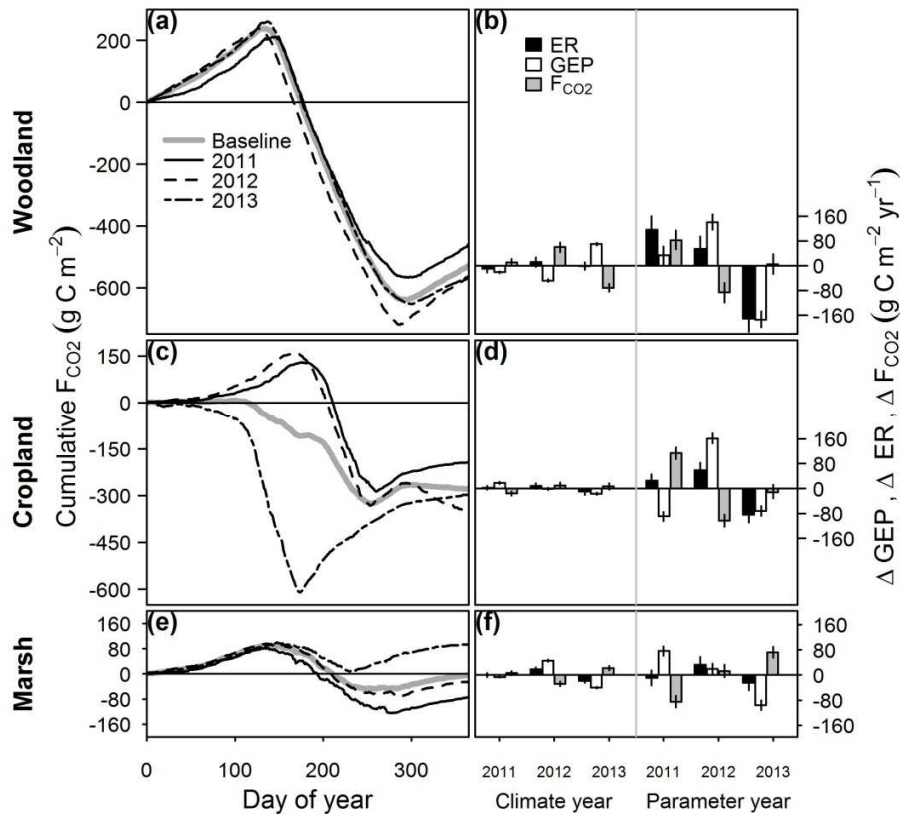
Fig. 7. Annual cumulative net ecosystem CO_2 exchange (F_{CO2}) (a, c, e) and the effects of environmental drivers (climate year) and model parameters (parameter year) (b, d, f) on annual F_{CO2} (ΔF_{CO2}), gross ecosystem production (ΔGEP), and ecosystem respiration (ΔER). The baseline F_{CO2} was obtained from the average of nine-scenario simulations at each site (Fig. 7a, c, e) and then used as the reference level (i.e., 0) in presenting the direct and indirect effects in Fig. 7b, d, f. The sign convention in Fig. 7b, d, f is that a positive effect on ER and GEP increases the respiration loss and assimilation uptake whereas a negative effect on F_{CO2} increases the net ecosystem CO_2 uptake. The effects that are caused by the interactions between the climate and parameter years are generally minor and are not presented here. Vertical segments in Fig. 7b, d, f showed the 95% quantile intervals of model simulation.

30

4. Discussion

4.1. Direct Climatic and Indirect Parameter Effects

Our findings reiterate the important roles of functional changes in driving the interannual F_{CO2} variability (i.e., indirect effect). Most importantly, the relative contribution of indirect effects could differ distinctly among sites, which leads to the cross-site difference of interannual F_{CO2} variability. While several studies have attempted to address the similar research questions (Hui et al., 2003; Polley et al., 2008; Richardson et al., 2007; Shao et al., 2014; Teklemariam et al., 2010; Wu et al., 2012), very few of them were conducted using such a cluster-wise experiment design. Thus, previous studies often constrained their scopes on either the long-term variability in one single site (e.g., Richardson et al., 2007; Wu et al., 2012) or a generalized overview of multiple sites from diverse climate zones and geo-locations (e.g., Shao et al., 2014; Shao et al., 2015). Often, those multi-site studies had to ignore the details of site-specific climatic conditions and the comparisons were carried out on simple metrics derived at the annual to interannual scales. The discrepancy in model structures further limited the capability in interpreting the varied results among studies.

In our case, we were able to partition the interannual variation at both the local and annual scales and examine the partitioned effects through times and across sites. Our study clearly showed that different ecosystems responded differently to such similar climatic forcing. The interannual F_{CO2} variability was larger (79 and 86 g C m^{-2} yr^{-1}) and dominated by indirect effects (89% and 86%) at the cropland and marsh sites. On the other hand, the interannual F_{CO2} variability and indirect effect were marginally lower at the woodland site (61 g C m^{-2} yr^{-1} and 54%). Our findings concurred with the proposition in Shao et al. (2015) that the cross-site difference of interannual F_{CO2} variability was largely determined by the difference of indirect

31

543   effects among sites.

544   To date, there is no consensus of what leads to the difference of the contribution of

545   indirect effects across sites. We argue that the histories and regimes (e.g., intensity, frequency) of

546   natural and human disturbance may explain at least a portion of the cross-site difference. Polley

547   et al. (2008) examined the interannual F_{CO2} variability at two nearby prairie sites with different

548   grazing management (grazed *vs.* ungrazed). They found that grazing management reduced the

549   influence of plants on ecosystem carbon processes. For example, it reduced the F_{CO2} variability

550   generated by plant physiological and phenological changes and it altered the most relevant

551   environmental drivers in explaining the F_{CO2} variability. A similar conclusion was made in

552   McVeigh et al. (2014) and Teklemariam et al. (2010), where ecosystems mediated the response

553   of CO_2 fluxes to climatic variability through a different degree of structural and functional

554   modification in the dominant vegetation. Teklemariam et al. (2010) argued that the difference

555   among ecosystems may be attributed to their different histories of natural and human

556   disturbance. The interannual F_{CO2} variability tends to be mainly driven by external environmental

557   variability in ecosystems that adjust to prolonged exposure of a given environmental condition,

558   such as the 70-year-old woodland in our study. In contrast, ecosystems that are prone to frequent

559   disturbance and management, such as the cropland in our case, tend to have the interannual F_{CO2}

560   variability mainly driven by indirect effects.

561   Further research should focus on generating a suitable framework to better quantify the

562   effects of the disturbance history and regime. Shao et al. (2015) argued that higher disturbance

563   intensity may not always lead to higher contribution of indirect effects. Different disturbance

564   regimes may also influence the interplay of direct and indirect effects. Currently, the data are still

565   insufficient to draw a general conclusion about the influence of disturbance regimes. Further

32

566   studies with a more sophisticated design (e.g., paired or cluster-wise sites) are required in order

567   to disentangle the explicit roles of disturbance regimes.

568   While the importance of indirect (or biotic/parameter) effects on interannual F_{CO2}

569   variability has been discussed in several studies (Hui et al., 2003; Polley et al., 2008; Richardson

570   et al., 2007; Shao et al., 2014; Teklemariam et al., 2010; Wu et al., 2012), challenges remain in

571   synthesizing these reports and interpreting the indirect effects. Extra caution is required because

572   different statistical models are adopted in partitioning the direct/indirect effects. Those models

573   are fundamentally different in their structure and/or statistical assumptions. Thus, the different

574   partitioned variation among reports reflects to an unknown extent the inherent model differences

575   (Shao et al., 2015; Wu et al., 2012). Potentially, the indirect effects involve the changes of

576   structural, physiological, and phenological traits of ecosystems (Humphreys and Lafleur, 2011;

577   Luo et al., 2001; Richardson et al., 2010). Different models may or may not be capable of

578   replicating the variation as induced by all those changes.

579   Additionally, unaccounted environmental drivers or prolonged and lagged effects that

580   were not incorporated in the model structure may also contribute to the indirect effects (Ciais et

581   al., 2005; Desai, 2014). Contrary to other studies (Baldocchi et al., 2005; Richardson et al.,

582   2007), we did not use soil temperature as a predictor variable in modeling the spring recovery

583   and fall senescence of GEP and ER. By incorporating soil temperature, a portion of the current

584   indirect effects at the woodland and marsh sites could be partitioned into the direct effects of soil

585   temperature (Fig. A.4). Interestingly, the strong relationship between the EVI and A_{max}/R_{ref}

586   suggested a potential avenue for further model improvement. Currently, challenges remain in

587   adequately incorporating these snap-shot/satellite-based vegetation indices (e.g., every 8 to 16

588   days) into our model framework. We suggest future studies should incorporate near-surface

589   continuous phenological measurements (e.g., radiometric sensors, digital cameras) (Ryu et al.,

590   2012; Soudani et al., 2012; Toomey et al., 2015). Thus, the changes in plant phenology can be

591   directly incorporated as predictor variables and the phenological effects can be distinguished

592   from the current indirect effects.

593

594   4.2. Influence of Climatic Variability and Anomaly

595   Recent climatic variability and anomalies in the Great Lakes region provided us a rare and

596   valuable opportunity to examine the interannual F_{CO_2} variability across different ecosystems.

597   With these record-breaking climate anomalies, we were able to examine how ecosystem carbon

598   processes may respond to the extreme and contrasting climatic conditions (e.g., wet-dry, warm-

599   cool) in a relative short time span (~3 years). Most importantly, the similar climatic variability

600   across the region allowed us to closely and simultaneously examine the response of F_{CO_2}

601   variability in different ecosystems. In general, the year-to-year changes of GEP and ER

602   correlated positively with each other when pooling all the site-year data (i.e., high annual GEP

603   with high annual ER) (Cor: 0.73; Fig. A.5a). The positive correlation is of great importance

604   because it implies that year-to-year variation of GEP and ER partly compensate each other,

605   which dampens the interannual variability of F_{CO_2} (Baldocchi, 2008). The year-to-year changes

606   of GEP and ER did not synchronize across sites (to be discussed below), suggesting that different

607   ecosystems responded differently to similar climate conditions in a specific year. We did not find

608   evident correlations between the direct and indirect effects as reported in Shao et al. (2014) (Fig.

609   A.5b, d, f). This lack of correlation suggests that ecosystem functional changes may not always

610   compensate or supplement the direct/instantaneous effects driven by environmental forcing

611   (neither synergistically nor antagonistically) (Richardson et al., 2007; Shao et al., 2014).

612   Both the woodland and cropland sites had the highest net CO_2 uptake in the warm year of

613   2012 mainly because of longer peak assimilation periods and higher assimilation potentials. The

614   marsh, in contrast, had lower net CO_2 uptake in 2012 than in 2011 because the increase of ER

615   exceeded the increase of GEP. Contrasting effects of an earlier warm spring on net annual CO_2

616   uptakes were reported in several studies across a diverse range of ecosystems in boreal and

617   temperate regions (e.g., Hu et al., 2010; Kross et al., 2014; Lafleur and Humphreys, 2008;

618   Richardson et al., 2009; Richardson et al., 2010). At the woodland site, the warm temperature in

619   2012 had the most influence through triggering earlier onsets of active/peak assimilation periods

620   and leading to higher annual assimilation potentials. Similar findings were reported in previous

621   studies showing that warm springs tend to enhance GEP more than ER in forest ecosystems

622   (Black et al., 2000; Richardson et al., 2010).

623   On the other hand, the net CO_2 uptake in wetlands may not always benefit from a warmer

624   climate condition (Sulman et al., 2010). As wetlands often accumulate a substantial amount of

625   carbon from allochthonous and autochthonous sources, the increase of ER may exceed the

626   increase of GEP during the warm years when more labile carbon becomes available for

627   decomposition as a consequence of a relatively lower water table (Chu et al., 2015; Lafleur et al.,

628   2003). Similarly, the effects of the warm spring on CO_2 uptake in croplands are less clear

629   because the planting schedule is often determined based on more than just one single factor (i.e.,

630   soil temperature). In our case, both the warm temperature and relatively low precipitation during

631   April–May (and thus adequate soil water status) in the 2012 spring provided favorable conditions

632   for early cultivation. Thus, soybeans were planted ~20 days earlier in 2012 than that in 2011,

633   when frequent precipitation led to near-saturated soil water content postponing the cultivation

634   schedule.

635   The cool spells in the 2013 summer influenced the marsh CO_2 uptake via reducing the

636 assimilation potential and GEP. The woodland site, in contrast, had slightly higher annual CO_2

637 uptake than the three-year average as a consequence of reduced ER. We found that the cool

638 events triggered early senescence and caused the peak assimilation period to end much earlier in

639 2013 at the marsh than in 2011 or 2012. The mechanisms of the cool-spell effects remain unclear

640 and have not been reported in previous wetland studies. In general, lower temperature led to

641 earlier senescence, which explained a large portion of the observed lower GEP. However, we

642 found that the response curves of A_{max} and R_{ref} against soil temperature in 2013 deviated from

643 those in 2011 or 2012, suggesting that other factors (e.g., chilling damage) may also play an

644 important role.

645

646 **5. Conclusions**

647 With only three years of data, we are cautious about drawing a generalized conclusion about the

648 interannual variability and long-term baseline of CO_2 fluxes at the three ecosystems. However,

649 the simultaneous CO_2 flux observation at multiple ecosystems that experienced similar climate

650 variability and anomaly certainly provide valuable insights in how contrasting ecosystems may

651 respond to similar environmental forcing. The positive correlation between the year-to-year

652 changes of GEP and ER suggests that GEP and ER generally compensate each other to a large

653 extent, leading to a decrease in the climate sensitivity of interannual F_{CO2}. Such co-varying GEP-

654 ER pattern is largely driven by nearly synchronous changes in the indirect effects of GEP and

655 ER. Thus, even when climate conditions vary drastically in our three-year study period, the

656 variability of the annual F_{CO2} (SD: 61–86 g C m^{-2} yr^{-1}) is still conservative and within the

657 reported ranges from cross-site/cross-year synthesis.

658   Our findings also highlight that changes in functional parameters (e.g., A_{max}, R_{ref}) over

659 the years play an important role in driving the interannual F_{CO_2} variability (54–89%) at all the

660 sites. The year-to-year changes of GEP/ER did not synchronize across sites. Consequently,

661 different ecosystems may respond differently to similar climatic conditions in a specific year in

662 terms of annual net CO_2 uptakes. While the warm temperature in the spring of 2012 triggered the

663 growing season in the woodland site to start earlier and substantially increased the annual CO_2

664 uptakes, similar conditions turned the marsh to near CO_2 neutral because of enhanced ER.

665 Similarly, the cool spell in the summer of 2013 also influenced GEP and ER differently in

666 different ecosystems that responded oppositely in their annual CO_2 uptake. Future research

667 should focus on the unequal response among ecosystems to similar climatic variability in order

668 to better predict, upscale, and assess the potential impacts of future climate change.

Appendix A. Implications of the Modeling Approach

Our attempts to utilize a structurally simple and flexible Bayesian hierarchical model provide insights into future ER-GEP modeling. First, the observed time series of F_{CO_2} is often composed of processes at multiple temporal scales (e.g., hourly, diurnal, synoptic, seasonal, interannual) (Baldocchi et al., 2001; Ouyang et al., 2014; Stoy et al., 2005). The superimposed characteristics pose challenges in constructing a suitable model that can duplicate and predict the carbon fluxes across a wide range of temporal scales (Desai, 2014). Often, the time series has to be divided and grouped according to the target scales (e.g., by year, by season) and fitted with separate sets of model parameters. In this case, the groups are treated independently and the unaccounted linkages among groups (e.g., among years, among seasons) often require extra works and caution in interpreting the modeling results.

The Bayesian hierarchical model takes advantages of linking the yearly parameters through higher level distributions (i.e., global) such that the year-to-year variation can be adequately described in the model structures and the overall estimate can be improved via sharing the information among years (Efron and Morris, 1977). Additionally, the seasonal and short-term (e.g., multi-daily or synoptic) dynamics of A_{max} and R_{ref} can be adequately described by using the prescribed empirical functions and random error structures. In our preliminary tests, we ran an additional model estimation by setting A_{max} and R_{ref} as a random-walk process, where A_{max} and R_{ref} were allowed to vary everyday through the time series while all other model structures were kept the same. We found that the random-walk model approach generated very similar seasonal and multi-daily dynamics in A_{max} and R_{ref} comparing to our current model (data not shown). This suggests that the current model structure was flexible and sufficient to capture the multi-scaled dynamics of CO_2 fluxes.

703   Second, the empirical phenological model we adopted provided an alternative approach

704   in quantifying the GEP/ER phenology and thus in simulating the seasonality of CO_2 fluxes.

705   Despite the fact that different equations were adopted, several previous studies have

706   demonstrated that the phenological modeling approach was informative, practical, and flexible

707   (e.g., Gu et al., 2003; Gu et al., 2009; Klosterman et al., 2014; Noormets et al., 2009; Toomey et

708   al., 2015). Once these models were estimated, the first and second derivate could be calculated

709   and a series of informative phenological indices could be determined along with properly-

710   defined uncertainty intervals (e.g., Fig. A.3). These mathematical characteristics make it feasible

711   to draw statistical inference from the cross-site or cross-year comparison (Noormets et al., 2009).

712   It was also noticeable that most previous studies used daily maxima or integrals while

713   fitting the phenological models (Gu et al., 2003; Gu et al., 2009; Noormets et al., 2009). We

714   showed that our Bayesian hierarchical model could serve as an alternative approach in estimating

715   the phenological indices. By using the half-hourly F_{CO2} directly, such approach reduces the

716   uncertainties that potentially originate from the gap-filling and/or GEP-ER partitioning

717   procedures. Also, the short-term effects of environmental forcing, such as PAR/VPD on GEP and

718   T_a/VWC on ER, can be explicitly incorporated into models. This helps eliminate the effects of

719   short-term environmental forcing and provides better estimates of the potential GEP and ER.

720   **References**

721   Ault, T. et al., 2013. The false spring of 2012, earliest in north American record. EOS,
722   Transactions American Geophysical Union, 94(20): 181-182.
723   Baldocchi, D.D. et al., 2001. A spectral analysis of biosphere-atmosphere trace gas flux densities
724   and meteorological variables across hour to multi-year time scales. Agric For Meteorol,
725   107(1): 1-27.
726   Baldocchi, D.D. et al., 2005. Predicting the onset of net carbon uptake by deciduous forests with
727   soil temperature and climate data: a synthesis of FLUXNET data. Int J Biometeorol,
728   49(6): 377-387.
729   Baldocchi, D.D., 2008. Turner review No. 15.'Breathing' of the terrestrial biosphere: lessons
730   learned from a global network of carbon dioxide flux measurement systems. Australian
731   Journal of Botany, 56(1): 1-26.
732   Baldocchi, D.D., 2014. Measuring fluxes of trace gases and energy between ecosystems and the
733   atmosphere—the state and future of the eddy covariance method. Global Change Biol,
734   20: 3600–3609.
735   Barr, A.G. et al., 2004. Inter-annual variability in the leaf area index of a boreal aspen-hazelnut
736   forest in relation to net ecosystem production. Agric For Meteorol, 126(3): 237-255.
737   Barr, A.G. et al., 2009. Climate and phenological controls of the carbon and energy balances of
738   three contrasting boreal forest ecosystems in western Canada. In: A. Noormets (Editor),
739   Phenology of Ecosystem Processes: Applications in Global Change Research. Springer,
740   New York, USA, pp. 3-34.
741   Black, T. et al., 2000. Increased carbon sequestration by a boreal deciduous forest in years with a
742   warm spring. Geophys Res Lett, 27(9): 1271-1274.
743   Bloom, A.A. and Williams, M., 2015. Constraining ecosystem carbon dynamics in a data-limited
744   world: integrating ecological "common sense" in a model–data fusion framework.
745   Biogeosciences, 12(5): 1299-1315.
746   Braswell, B. et al., 1997. The response of global terrestrial ecosystems to interannual temperature
747   variability. Science, 278(5339): 870-873.
748   Brooks, S.P. and Gelman, A., 1998. General methods for monitoring convergence of iterative
749   simulations. Journal of Computational and Graphical Statistics, 7(4): 434-455.
750   Carbone, M.S. et al., 2008. Soil respiration in perennial grass and shrub ecosystems: linking
751   environmental controls with plant and microbial sources on seasonal and diel timescales.
752   Journal of Geophysical Research: Biogeosciences, 113(G2): G02022.
753   Chu, H. et al., 2014. Net ecosystem methane and carbon dioxide exchanges in a Lake Erie
754   coastal marsh and a nearby cropland. Journal of Geophysical Research: Biogeosciences,
755   119(5): 722-740.
756   Chu, H. et al., 2015. Climatic variability, hydrologic anomaly, and methane emission can turn
757   productive freshwater marshes into net carbon sources. Global Change Biol, 21(3): 1165-
758   1181.
759   Ciais, P. et al., 2005. Europe-wide reduction in primary productivity caused by the heat and
760   drought in 2003. Nature, 437(7058): 529-533.
761   Cook, B.D. et al., 2004. Carbon exchange and venting anomalies in an upland deciduous forest
762   in northern Wisconsin, USA. Agric For Meteorol, 126(3–4): 271-295.
763   Cox, P.M. et al., 2000. Acceleration of global warming due to carbon-cycle feedbacks in a
764   coupled climate model. Nature, 408(6809): 184-187.

765   DeForest, J. et al., 2006. Phenophases alter the soil respiration–temperature relationship in an
766   oak-dominated forest. Int J Biometeorol, 51(2): 135-144.

767   DeForest, J. et al., 2009. Leaf litter is an important mediator of soil respiration in an oak-
768   dominated forest. Int J Biometeorol, 53(2): 127-134.

769   Desai, A.R., 2010. Climatic and phenological controls on coherent regional interannual
770   variability of carbon dioxide flux in a heterogeneous landscape. Journal of Geophysical
771   Research: Biogeosciences, 115(G3): G00J02.

772   Desai, A.R., 2014. Influence and predictive capacity of climate anomalies on daily to decadal
773   extremes in canopy photosynthesis. Photosynth Res, 119(1-2): 31-47.

774   Efron, B. and Morris, C.N., 1977. Stein's paradox in statistics. Scientific American, 236(5): 119-
775   127.

776   Falge, E. et al., 2001. Gap filling strategies for defensible annual sums of net ecosystem
777   exchange. Agric For Meteorol, 107(1): 43-69.

778   Gouhier, T., 2014. biwavelet: Conduct univariate and bivariate wavelet analyses (Version 0.14).

779   Grinsted, A. et al., 2004. Application of the cross wavelet transform and wavelet coherence to
780   geophysical time series. Nonlinear Processes in Geophysics, 11: 561-566.

781   Gu, L. et al., 2003. Phenology of Vegetation Photosynthesis. In: M.D. Schwartz (Editor),
782   Phenology: An Integrative Environmental Science. Tasks for Vegetation Science. Kluwer
783   Academic Publishers, Netherlands, pp. 467-485.

784   Gu, L. et al., 2009. Characterizing the seasonal dynamics of plant community photosynthesis
785   across a range of vegetation types. In: A. Noormets (Editor), Phenology of Ecosystem
786   Processes: Applications in Global Change Research. Springer New York, USA, pp. 35-
787   58.

788   Heimann, M. and Reichstein, M., 2008. Terrestrial ecosystem carbon dynamics and climate
789   feedbacks. Nature, 451(7176): 289-292.

790   Hu, J. et al., 2010. Longer growing seasons lead to less carbon sequestration by a subalpine
791   forest. Global Change Biol, 16(2): 771-783.

792   Hui, D. et al., 2003. Partitioning interannual variability in net ecosystem exchange between
793   climatic variability and functional change. Tree Physiology, 23(7): 433-442.

794   Humphreys, E.R. and Lafleur, P.M., 2011. Does earlier snowmelt lead to greater CO2
795   sequestration in two low Arctic tundra ecosystems? Geophys Res Lett, 38(9): L09703.

796   Jarvis, P. et al., 2007. Drying and wetting of Mediterranean soils stimulates decomposition and
797   carbon dioxide emission: the "Birch effect". Tree Physiology, 27(7): 929-940.

798   Karl, T.R. et al., 2012. U.S. temperature and drought: Recent anomalies and trends. EOS,
799   Transactions American Geophysical Union, 93(47): 473.

800   Klosterman, S.T. et al., 2014. Evaluating remote sensing of deciduous forest phenology at
801   multiple spatial scales using PhenoCam imagery. Biogeosciences, 11(16): 4305-4320.

802   Knudson, W.A., 2012. The economic impact of the this spring's weather on the fruit and
803   vegetable sectors. The Strategyic Marketing Institute, Michigan State University, East
804   Lansing, MI, USA.

805   Kross, A.S.E. et al., 2014. Phenology and its role in carbon dioxide exchange processes in
806   northern peatlands. Journal of Geophysical Research: Biogeosciences, 119(7): 1370-
807   1384.

808   Lafleur, P.M. et al., 2003. Interannual variability in the peatland-atmosphere carbon dioxide
809   exchange at an ombrotrophic bog. Global Biogeochem Cy, 17(2): 1036.

810   Lafleur, P.M. and Humphreys, E.R., 2008. Spring warming and carbon dioxide exchange over

811   low Arctic tundra in central Canada. Global Change Biol, 14(4): 740-756.

812 Lasslop, G. et al., 2010. Separation of net ecosystem exchange into assimilation and respiration
813   using a light response curve approach: critical issues and global evaluation. Global
814   Change Biol, 16(1): 187-208.

815 Lloyd, J. and Taylor, J.A., 1994. On the temperature dependence of soil respiration. Functional
816   Ecology, 8(3): 315-323.

817 Luo, Y. et al., 2001. Acclimatization of soil respiration to warming in a tall grass prairie. Nature,
818   413(6856): 622-625.

819 Luo, Y. et al., 2009. Terrestrial carbon‐cycle feedback to climate warming: experimental
820   evidence on plant regulation and impacts of biofuel feedstock harvest. Global Change
821   Biology: Bioenergy, 1(1): 62-74.

822 McVeigh, P. et al., 2014. Meteorological and functional response partitioning to explain
823   interannual variability of CO_2 exchange at an Irish Atlantic blanket bog. Agric For
824   Meteorol, 194(0): 8-19.

825 Melillo, J.M. et al. (Editors), 2014. Climate Change Impacts in the United States: The Third
826   National Climate Assessment. U.S. Global Change Research Program, Washington, DC.
827   USA.

828 Moffat, A.M. et al., 2007. Comprehensive comparison of gap-filling techniques for eddy
829   covariance net carbon fluxes. Agric For Meteorol, 147(3-4): 209-232.

830 Morisette, J.T. et al., 2008. Tracking the rhythm of the seasons in the face of global change:
831   phenological research in the 21st century. Frontiers in Ecology and the Environment,
832   7(5): 253-260.

833 Noormets, A. et al., 2008a. Moisture sensitivity of ecosystem respiration: Comparison of 14
834   forest ecosystems in the Upper Great Lakes Region, USA. Agric For Meteorol, 148(2):
835   216-230.

836 Noormets, A. et al., 2008b. Drought during canopy development has lasting effect on annual
837   carbon balance in a deciduous temperate forest. New Phytologist, 179(3): 818-828.

838 Noormets, A. et al., 2009. The phenology of gross ecosystem productivity and ecosystem
839   respiration in temperate hardwood and conifer chronosequences. In: A. Noormets
840   (Editor), Phenology of Ecosystem Processes: Applications in Global Change Research.
841   Springer, New York, USA, pp. 59-85.

842 Ollinger, S. et al., 2008. Canopy nitrogen, carbon assimilation, and albedo in temperate and
843   boreal forests: Functional relations and potential climate feedbacks. Proceedings of the
844   National Academy of Sciences, 105(49): 19336-19341.

845 Ouyang, Z. et al., 2014. Disentangling the confounding effects of PAR and air temperature on net
846   ecosystem exchange at multiple time scales. Ecological Complexity, 19: 46-58.

847 Papale, D. et al., 2006. Towards a standardized processing of net ecosystem exchange measured
848   with eddy covariance technique: Algorithms and uncertainty estimation. Biogeosciences,
849   3(4): 571-583.

850 Plummer, M., 2003. JAGS: A program for analysis of Bayesian graphical models using Gibbs
851   sampling. In: K. Hornik et al. (Editors), Proceedings of the 3rd International Workshop
852   on Distributed Statistical Computing, Vienna, Austria.

853 Plummer, M. et al., 2006. CODA: Convergence diagnosis and output analysis for MCMC. R
854   News, 6: 7-11.

855 Polley, H.W. et al., 2008. Interannual variability in carbon dioxide fluxes and flux-climate
856   relationships on grazed and ungrazed northern mixed-grass prairie. Global Change Biol,

14(7): 1620-1632.

Reichstein, M. et al., 2005. On the separation of net ecosystem exchange into assimilation and ecosystem respiration: review and improved algorithm. Global Change Biol, 11(9): 1424-1439.

Richardson, A.D. et al., 2006. A multi-site analysis of random error in tower-based measurements of carbon and energy fluxes. Agric For Meteorol, 136(1-2): 1-18.

Richardson, A.D. et al., 2007. Environmental variation is directly responsible for short- but not long-term variation in forest-atmosphere carbon exchange. Global Change Biol, 13(4): 788-803.

Richardson, A.D. et al., 2009. Influence of spring phenology on seasonal and annual carbon balance in two contrasting New England forests. Tree Physiology, 29(3): 321-331.

Richardson, A.D. et al., 2010. Influence of spring and autumn phenological transitions on forest ecosystem productivity. Philosophical Transactions of the Royal Society B: Biological Sciences, 365(1555): 3227-3246.

Ryu, Y. et al., 2012. Continuous observation of tree leaf area index at ecosystem scale using upward-pointing digital cameras. Remote Sensing of Environment, 126: 116-125.

Sala, A. et al., 2010. Physiological mechanisms of drought‐induced tree mortality are far from being resolved. New Phytologist, 186(2): 274-281.

Shao, J. et al., 2014. Partitioning climatic and biotic effects on interannual variability of ecosystem carbon exchange in three ecosystems. Ecosystems, 17(7): 1186-1201.

Shao, J. et al., 2015. Biotic and climatic controls on interannual variability in carbon fluxes across terrestrial ecosystems. Agric For Meteorol, 205(0): 11-22.

Shi, Z. et al., 2014. Differential effects of extreme drought on production and respiration: synthesis and modeling analysis. Biogeosciences, 11(3): 621-633.

Solymos, P., 2010. dclone: Data cloning in R. The R Journal, 2(2): 29-37.

Soudani, K. et al., 2012. Ground-based Network of NDVI measurements for tracking temporal dynamics of canopy structure and vegetation phenology in different biomes. Remote Sensing of Environment, 123(0): 234-245.

Sowerby, A. et al., 2005. Microbial community changes in heathland soil communities along a geographical gradient: interaction with climate change manipulations. Soil Biology and Biochemistry, 37(10): 1805-1813.

Stoy, P.C. et al., 2005. Variability in net ecosystem exchange from hourly to inter-annual time scales at adjacent pine and hardwood forests: a wavelet analysis. Tree Physiology, 25(7): 887-902.

Stoy, P.C. et al., 2013. Evaluating the agreement between measurements and models of net ecosystem exchange at different times and timescales using wavelet coherence: an example using data from the North American Carbon Program Site-Level Interim Synthesis. Biogeosciences, 10(11): 6893-6909.

Sulman, B.N. et al., 2010. CO_2 fluxes at northern fens and bogs have opposite responses to inter-annual fluctuations in water table. Geophys Res Lett, 37(19): L19702.

Teklemariam, T.A. et al., 2010. The direct and indirect effects of inter-annual meteorological variability on ecosystem carbon dioxide exchange at a temperate ombrotrophic bog. Agric For Meteorol, 150(11): 1402-1411.

Thibault, K.M. and Brown, J.H., 2008. Impact of an extreme climatic event on community assembly. Proceedings of the National Academy of Sciences of the United States of America, 105(9): 3410-3415.

903   Tierney, L. et al., 2009. Snow: A parallel computing framework for the R system. International
904   Journal of Parallel Programming, 37(1): 78-90.
905   Toomey, M. et al., 2015. Greenness indices from digital cameras predict the timing and seasonal
906   dynamics of canopy-scale photosynthesis. Ecol Appl, 25(1): 95-115.
907   Wu, J. et al., 2012. Effects of climate variability and functional changes on the interannual
908   variation of the carbon balance in a temperate deciduous forest. Biogeosciences, 9: 13-28.
909   Wuebbles, D.J. et al., 2014. Severe weather in United States under a changing climate. EOS,
910   Transactions American Geophysical Union, 95(18): 149-150.
911   Xiao, J. et al., 2010. A continuous measure of gross primary production for the conterminous
912   United States derived from MODIS and AmeriFlux data. Remote Sensing of
913   Environment, 114(3): 576-591.
914   Xie, J. et al., 2014. Long-term variability and environmental control of the carbon cycle in an
915   oak-dominated temperate forest. Forest Ecol Manag, 313: 319-328.
916   Xu, J. et al., 2011. Influence of timber harvesting alternatives on forest soil respiration and its
917   biophysical regulatory factors over a 5-year period in the Missouri Ozarks. Ecosystems,
918   14(8): 1310-1327.
919   Yi, C. et al., 2010. Climate control of terrestrial carbon exchange across biomes and continents.
920   Environ Res Lett, 5(3): 034007.
921   Zobitz, J. et al., 2011. A primer for data assimilation with ecological models using Markov Chain
922   Monte Carlo (MCMC). Oecologia, 167(3): 599-611.